Development of Multi-Radioisotope Identification Algorithm Using an Artificial Neural Network for Plastic Gamma Spectra

Jinhwan Kim [a], Wooseub Kim [a], Gyuseong Cho [a*]
[a]*Department of Nuclear & Quantum Engineering, Korea Advanced Institute of Science and Technology, 291 Daehak-ro, Yuseong-gu, Daejeon, 305-701, Republic of Korea*
[*]*Corresponding author: gscho@kaist.ac.kr*

1. Introduction

Radiation portal monitors (RPMs) were deployed at ports and airports to prevent contaminated or illicit radioactive materials from entering Korea. When RPMs generate alarms based on net counts above a certain threshold, additional detection by a field-portable detector, such as NaI(Tl) or cadmium zinc telluride (CZT), need to be carried out to identify the radioisotopes with high precision [1]. However, these detectors are expensive and sensitive to temperature variations. Plastic scintillators are economical and have the characteristic of near temperature independence with a variation of about 1% between 0 and 50 ℃ [2], but they are rarely used for radioisotope identification because of the overlapping of the broad Compton continuum and loss in photopeaks.

In this paper, we propose an algorithm to identify multi radioisotopes as well as a single radioisotope based on plastic gamma spectra. The four radioisotopes ^{22}Na, ^{137}Cs, ^{60}Co, and ^{54}Mn were used and a total of 16 classes with those combinative radioisotopes were labeled, as shown in Figure 1. Spectra were simulated by the Monte Carlo N-Particle transport code 6 (MCNP6) [3] to create the training set. Spectra were measured by a 2-inch EJ-200 to create validation and test sets. Python package Keras [4] was used to train the ANN presented in this paper.

Class	1	2	3	4	5	6	7	8	9	10	11	12	13	14	15	16
Background	O	O	O	O	O	O	O	O	O	O	O	O	O	O	O	O
^{22}Na		O				O	O	O				O	O	O		O
^{137}Cs			O			O			O	O		O	O		O	O
^{60}Co				O			O		O		O	O		O	O	O
^{54}Mn					O			O		O	O		O	O	O	O

Fig. 1. Total 16 classes with the four combinative radioisotopes.

2. Methods and methods

2.1 Training set creation

To create the training set, the gamma spectra were simulated by the MCNP6 using a model of the EJ-200 scintillator. It was necessary to apply an "FT8 GEB" card to mimic a more realistic spectrum. The calculated values of "a," "b," and "c" coefficients through the full width at half maximum (FWHM) of measured spectra were used as input to the MCNP6 code based on a fitting function illustrated in Equation below where E is the incident gamma energy (MeV).

$$\mathrm{FWHM} = a + b\sqrt{E + cE^2}$$

We used three different types of GEB cards, namely GEB1, GEB2, and GEB3, to diversify the spectral resolution. The various spectra through these GEB cards prevent the overfitting issue that can occur in the ANN.

Figure 2 describes the architecture of creating the training set. Three hundred spectra were generated for each class. The radioisotope ratios of the spectra were randomly selected. Even though we indented to mimic the measured spectrum through simulation, there was a discrepancy in the low energy region due to backscattering by the surrounding structure and the background. In order to prevent the ANN from recognizing this difference as features of the class, 10 measured spectra corresponding to each class were included in the training set. To augment the number of spectra, a spectrum of 800 channels was extracted from the original spectrum of 1024 channels. This extraction was repeated 9 times within different ranges of the spectrum. All extracted data, which came to 44,550 spectra, were normalized and shuffled to be delivered to the ANN as the training set.

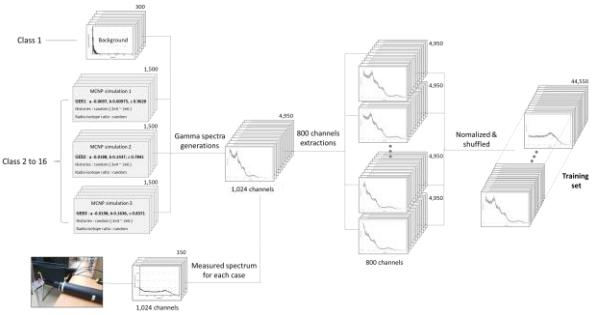

Fig. 2. Pretreatment architecture for training set creation.

2.2 Validation and Test sets creation

To create the validation and test sets, gamma spectra were measured for the 16 classes. Figure 3 describes the procedure for creating the two sets. For the test set, the sources were placed 1 cm, 5 cm and 10 cm apart from the detector (referred to as 1 cm apart, 5 cm apart and

10 cm apart, respectively) and were measured from 1 second to 10 seconds with intervals of 1 second. This procedure was repeated 3 times. Therefore, the number of the spectra with 1,024 channels in the test set came to 1,440. For the validation set, on the other hand, spectra were generated only for 10 cm apart and a spectrum of 800 channels was extracted in the same manner as in section 2.1. The number of the spectra in the validation set came to 1,440.

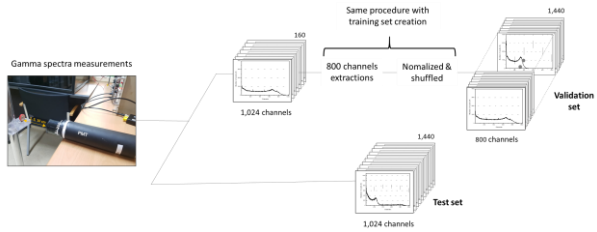

Fig. 3. The procedure for creating a validation set and a test set.

2.3 Radioisotope identification procedure

In this paper, we also propose a voting process to identify the radioisotopes, as illustrated in Figure 4. Different channels of spectra ranging from 40 to 840, 60 to 860, 80 to 880, 100 to 900, 120 to 920, 140 to 940, 160 to 960, 180 to 980, and 200 to 1,000 were extracted from the 1024 channel spectrum in the test set. These spectra were used as input data for the ANN. Furthermore, the final prediction was made by a vote based on the corresponding predictions.

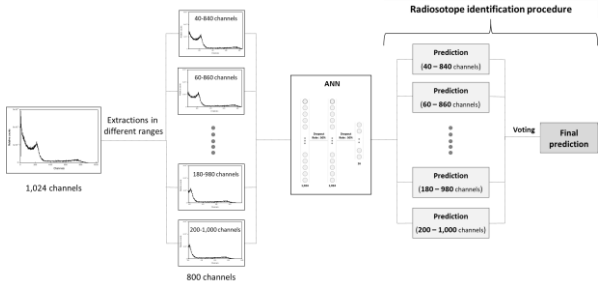

Fig. 4. Determination procedure for final predictions through voting.

2.4 Network architecture

The ANN presented in this paper consists of three fully-connected layers. An activation function then performs this summation, and the result is passed on to the next layer. In the proposed system, the input layer and the two hidden layers use rectified linear units (ReLUs) as activation functions because of their fast convergence on large datasets [5]. In the last layer, we used the softmax activation function to quantify the probability belonging to each class. In addition, back-propagation [6] using the Adam optimizer [7] adjusted the weights and bias to minimize the cross-entropy error.

3. Results and discussion

3.1 Network architecture

In this study, the performance for radioisotope identification was evaluated by the accuracy, which was defined as the ratio of the total number of accurately evaluated spectra to the total number of evaluated spectra. Figure 5 shows the accuracy of the ANN's calculation using the test sets. As shown in the figure, the proposed system had a high accuracy of 98.9% for the single radioisotope and 99.1% for the multi radioisotopes. Depending on the distance, it was 99%, 99.4%, and 97.9% for each of 1, 5, and 10cm apart, showing that it decreased slightly in the 10cm apart. This may have been a result of incorrect calculation due to a decrease in the counts of channels by low detection efficiency, which resulted in an increase in uncertainty and an increase in the background effect. Looking at the class, the accuracy was reduced in class 5, 10 cm apart, and all the cases in which class 4 was confirmed to be wrong were calculated as class 1 (background) due to the low counts of ^{54}Mn as shown in Figure 6 (a). However, it still had a high accuracy of 90.0%. For the reason mentioned earlier, some incorrectly calculated class 15 as class 9. As shown in Figure 6 (b), it is difficult to tell the difference when comparing the two spectra, but it could be classified as 93.0% accuracy. In addition, it showed 99.0% accuracy for the entire 1,440 spectra of the test set by separating all the similar spectra difficult to distinguish the characteristics of the radioisotopes, like Figures 6 (c) and (d).

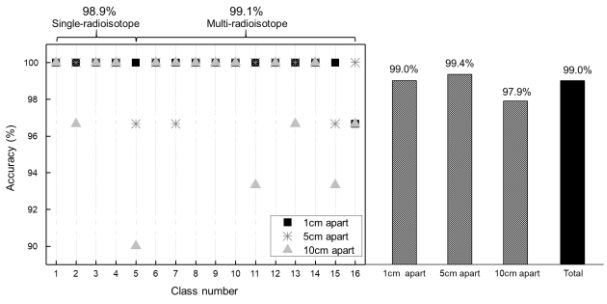

Fig. 5. The accuracy that ANN predicted using test sets. (Left) the accuracy according to the class, (right) the accuracy according to the distance.

In this study, voting procedures were developed to improve the identification accuracy, so training sets were organized through pretreatment processes. Figure 7 shows the comparison of accuracy in the different extracted ranges of the spectrum. From these results, it appears that accuracy through the voting process is higher than that of each channel range. In addition, considering that there is a deviation in the accuracy of

the channel ranges, it may be able to increase the reliability of the results by determining the overall results of various channel ranges. In this figure, the accuracy tends to decrease when the extracted channel range moves to a high energy. This is because the Compton maximum or continuum, which shows the characteristic of radioisotopes, appears below 1 MeV in most cases due to the characteristic of plastic scintillators in which photoelectric absorption rarely occurs. As the extracted channel range moves to a high energy, the spectrum loses such information, so the accuracy may decrease.

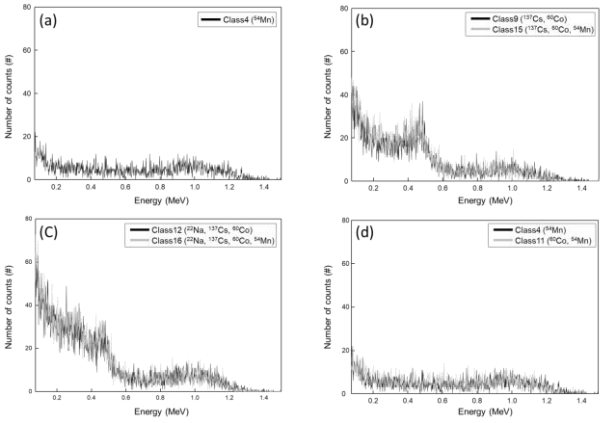

Fig. 6. An example of the test set that was correctly predicted by the ANN (10cm apart, 1 second).

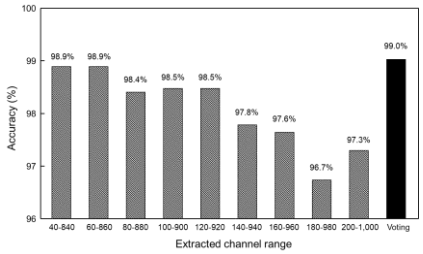

Fig. 7. The comparison of accuracy in the different extracted ranges of the spectrum and the accuracy through the voting procedures.

When creating the test sets, we included 10 measured spectra by class. This was to prevent the ANN from recognizing the difference between the simulated spectra and the measured spectra at less than 0.3 MeV as a characteristic of the class. Figure 8 shows the result of evaluating the accuracy of the test set after excluding the 150 measured spectra in the training set and setting the rest of the training process to be the same. As shown in the figure, the accuracy decreased to 81.5%. Adding just 10 measured spectra per class made it possible to improve the accuracy by 17.5%.

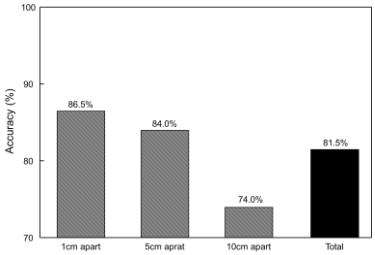

Fig. 8. The accuracy of the test set after excluding the 150 measured spectra in the training set.

3.2 Gain shift sensitivity performance

To study further the identification performance though plastic gamma spectra shifted by calibration drift or temperature, we shifted the spectra to 36 keV for each high energy and low energy, based on the response function of the scintillator to 0.662 MeV, by adjusting the gain (each is referred to as a positive bias and a negative bias). For each spectrum for the positive bias and the negative bias, respectively, the test sets were created by measuring each of the 1,440 spectra in the same way as for the method of creating test sets described in Section 2.2. These test sets were evaluated by the trained ANN. Figure 10 shows that the accuracy of the negative bias was 97.8%, showing that the accuracy was hardly reduced. On the other hand, when the spectra were biased to a high energy, the accuracy decreased to 85.0%. This is because increasing the gain not only shifts the spectra to a high energy, but also broadens the Compton continuum in the same spectral range, as shown in Figure 9. This means that the accuracy might be reduced due to the fact that the ANN has lacked training on broader spectra.

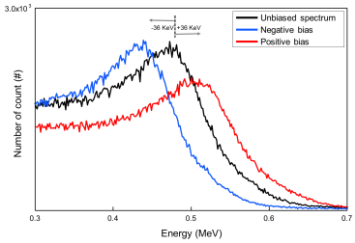

Fig. 9. Measurement spectra shifted by 36 keV for each high energy and low energy by adjusting the gain, based on the response function of the scintillator to 0.662 MeV.

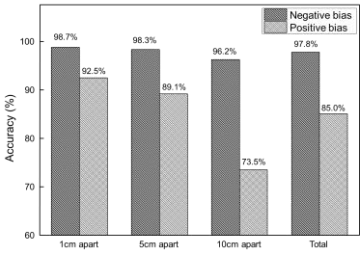

Fig. 10. The comparison of identification accuracy for the positive bias and negative bias.

3.3 Minimum identifiable activity

The question then arises: how can small activities of the radioisotopes be identified with the proposed algorithm? This may be related to the minimum identifiable activity (MIA) proposed by ORTEC [8]. In this study, we defined the "count quality factor" C as in Equation below to calculate the MIA with less than 5% of the FP and FN for the radioisotope where G represents the gross counts in a spectrum ranging from 40 to 1,000 channels, B is the number of background counts in the same region, and σ_N is the uncertainty of G-B.

$$C \equiv \frac{G - B}{\sigma_N}$$

C was calculated by measuring each radioisotope and background 200 times for 0.01, 0.02, 0.05, 0.1, 0.3, 0.5, 1, 2, 3, 5, and 1 seconds at 10cm apart. The FP showed a result of less than 5% for all calculated C ranges, but the FN becomes 5% or less at the values of C more than 38, 39, 142, and 30 in the radioisotopes of ^{22}Na, ^{137}Cs, ^{60}Co, and ^{54}Mn, respectively. Table Ⅰ shows the number of total net counts in the detector and the MIA in which C, FP, and FN are less than 5% by the radioisotope.

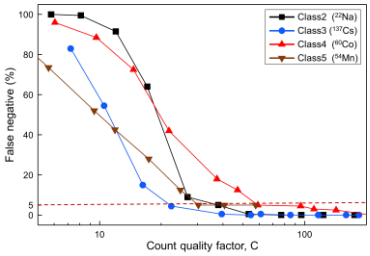

Fig. 11. FN variation according to changes in the value of C by class.

Table I. Total net counts in the detector and the calculated MIA in which FP and FN are less than 5% by the radioisotope.

Class	MIA (μ Ci)	Total net counts (#)
Class2 (^{22}Na)	6.4	1,538±40
Class3 (^{137}Cs)	6.7	508±22
Class4 (^{60}Co)	46.2	8,247±85
Class5 (^{54}Mn)	12.4	1,054±33

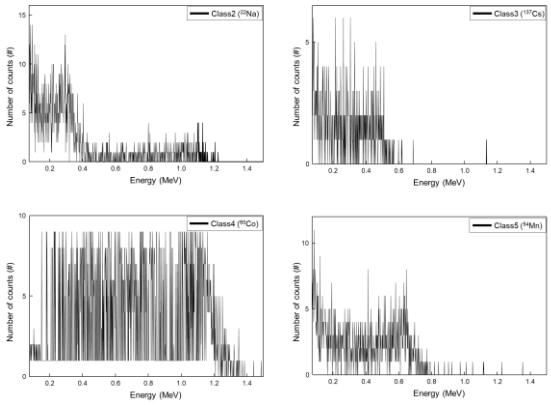

Fig. 12. Measured spectrum corresponding to the MIA by class.

3. Results and discussion

Previous studies were limited to identifying a single radioisotope because of the low photoelectric absorption and poor resolution of plastic scintillators, so no studies have been done to classify multi radioisotopes. However, we were able to focus on identifying multi radioisotopes as well as a single radioisotope by developing the ANN-based algorithm. It used some of the measured spectra during training as well as voting procedures to increase the accuracy of the results. In addition, the ANN was trained by extracting different channel ranges of spectra to improve the accuracy and reliability of the results even if the gain shift would occur in the spectra. we achieved an accuracy of 99.0% by applying the algorithm proposed in this study. This high accuracy was similar for the negative bias but was reduced to 85.0% for the positive bias. It is possible to identify the radioisotopes with less than 5% of the FP and FN even in the spectra with a high uncertainty due to a short spectral acquisition time.

REFERENCES

[1] R.C. Runkle, M.F. Tardiff, K.K. Anderson, D.K. Carlson, L.E. Smith, Analysis of Spectroscopic Radiation Portal Monitor Data Using Principal Components Analysis, IEEE Trans. Nucl. Sci. 53 (2006) 1418–1423.
[2] H. Search, C. Journals, A. Contact, M. Iopscience, I.P. Address, A.S. Beddar, T.R. Mackie, F.H. Attix, Characteristics and theoretical considerations Water-equivalent plastic scintillation detectors for high- energy beam dosimetry : I . Physical characteristics and theoretical considerations, Phys. Med. Biol. 37 (1992) 1883–1900.
[3] J.T. Goorley, M.R. James, T.E. Booth, F.B. Brown, J.S. Bull, L.J. Cox, J.W. Durkee, J.S. Elson, M.L. Fensin, R.A. Forster, J.S. Hendricks, H.G. Hughes, R.C. Johns, B.C. Kiedrowski, S.G. Mashnik, MCNP6 User's Manual, Version 1.0, Los Alamos Sci. Lab. (2013) 0–765.
[4] F. and others Chollet, Keras, GitHub. (2015). https://github.com/fchollet/keras.
[5] A. Krizhevsky, I. Sutskever, G.E. Hinton, ImageNet Classification with Deep Convolutional Neural Networks, Adv. Neural Inf. Process. Syst. (2012) 1–9.
[6] X.H. Yu, G.A. Chen, Efficient backpropagation learning using optimal learning rate and momentum, Neural Networks. 10 (1997) 517–527.
[7] D.P. Kingma, J. Ba, Adam: A Method for Stochastic Optimization, Int. Conf. Learn. Represent. (2015) 1–15.
[8] R.M. Keyser, F. Sergent, T.R. Twomey, D.L. Upp, A minimum detectable activity estimates for a germanium—detector based spectroscopic portal monitor, INMM 47th Annu. Meet. 2006. (2006).